RSC Advances

PAPER

View Article Online
View Journal | View Issue

Check for updates

Cite this: *RSC Adv.*, 2021, **11**, 3104

Re-dispersion of Pd-based bimetallic catalysts by hydrothermal treatment for CO oxidation†

Min Suk Choi, Hojin Jeong and Hyunjoo Lee *

Received 23rd November 2020
Accepted 7th January 2021

DOI: 10.1039/d0ra09912k

rsc.li/rsc-advances

The Pd/CeO_2 catalyst, which is highly active catalyst in automobile emission control especially for CO oxidation, often suffers from severe sintering under harsh condition, specifically hydrothermal treatment. Here, we report re-dispersion of Pd-based bimetallic (Pd–Fe, Pd–Ni, and Pd–Co) catalysts deposited on ceria by hydrothermal treatment at 750 °C using 10% H_2O. The re-dispersion was confirmed by various characterization techniques of transmission electron microscopy, CO chemisorption, CO-diffuse reflectance infrared Fourier transform, CO-temperature programmed desorption, and X-ray absorption spectroscopy. The dispersion of Pd increased significantly after hydrothermal treatment, resulting in improved CO oxidation activity. The presence of secondary transition metals enhanced the CO oxidation activity further, especially hydrothermally treated Pd–Fe bimetallic catalyst showed the highest activity for CO oxidation.

Open Access Article. Published on 13 January 2021. Downloaded on 2/8/2026 1:19:41 PM.
This article is licensed under a Creative Commons Attribution-NonCommercial 3.0 Unported Licence.

Introduction

In heterogeneous catalysis, supported metal catalysts have been studied in various directions, such as metal support interactions, confinement effects, and interface modification.[1–3] The difference in reactivity depends on the characteristics of the support. Various metal oxide materials, such as Al_2O_3, TiO_2, ZrO_2, and CeO_2, have been used as catalytic support because they strongly interact with metal atoms.[4] Especially, CeO_2-supported metal catalysts have showed high catalytic performance due to their high redox property, lattice oxygen mobility, and oxygen capacity.[5] CeO_2 easily donates the active lattice oxygen as the charge of cerium changes from Ce^{4+} to Ce^{3+}, which is useful in various oxidation reactions such as benzyl alcohol oxidation, ammonia oxidation, soot oxidation, and CO oxidation.[6–9]

In particular, CO oxidation is an important reaction in an automobile emission control system.[10,11] Emissions in gasoline engine and diesel engine vehicles contain substantial CO, NO_x, particulate matter (PM), and various hydrocarbons (C_xH_y). These pollutants should be converted into CO_2, N_2, and H_2O through the catalytic reactions. However, a large amount of pollutants are discharged at cold-start condition because the temperature of the engine is lower, resulting in lower temperatures in exhaust after-treatment system, often lower than the operation temperature of the catalyst.[12] Therefore, it is necessary to improve the catalytic activity at low temperature. Typically, precious metals such as Pt, Pd, and Rh have been used for pollution remediation in automobile exhaust. Especially, supported Pd catalysts have attracted a lot of attention for various chemical reactions such as oxidation, hydrogenation, dehydrogenation,[13–16] automobile emission control system.[17,18] However, because of the scarcity and high cost, the use efficiency and catalytic activity of Pd should be improved significantly.

To increase the utility of precious metals, the re-dispersion, which indicates the size decrease of metal nanoparticles after the certain treatment, has been reported. Nagai *et al.* showed that the oxidative treatment induced re-dispersion of Pt nanoparticles supported on CeZrY mixed oxide for automobile after-treatment.[19] Kaneko *et al.* reported that the effect of pretreatment conditions on the dispersion of Pt/SiO_2.[20] Dispersion of Pt species depends on calcination temperature of supported Pt precursor. Re-dispersed $PtCl_2$ species were obtained from decomposition of $PtCl_4$ by calcination at 375 °C. Jeong *et al.* reported the re-dispersion of Pd/CeO_2 catalyst after hydrothermal treatment, resulting in enhanced catalytic activity for CO oxidation.[21] The re-dispersion process using hydrothermal treatment is a non-toxic treatment process, and has the advantage of having similar condition with hydrothermal aging durability test in automobile catalysts.

To improve the activity and minimize the use of precious metals, various studies on bimetallic catalysts with non-precious transition metals have been performed. Yamamoto *et al.* reported Pt bimetallic catalyst using Cu and Ni on γ-Fe_2O_3 support. $Pt_{78}Cu_{22}$ and $Pt_{85}Ni_{15}$ showed the mostly improved CO oxidation activity.[22] Liu *et al.* reported computational DFT study about CO oxidation pathways when various second metals were added to CeO_2 supported Pd.[23] When Ag or Cu was added to Pd/CeO_2, CO was adsorbed on Pd site, but O_2 was adsorbed on Ag

Department of Chemical and Biomolecular Engineering, Korea Advanced Institute of Science and Technology, Daejeon 34141, South Korea. E-mail: azhyun@kaist.ac.kr; Tel: +82-42-350-3922

† Electronic supplementary information (ESI) available. See DOI: 10.1039/d0ra09912k

© 2021 The Author(s). Published by the Royal Society of Chemistry

Open Access Article. Published on 13 January 2021. Downloaded on 2/8/2026 1:19:41 PM.
This article is licensed under a Creative Commons Attribution-NonCommercial 3.0 Unported Licence.

or Cu site. The adsorption sites of CO and O_2 were separated, resulting in enhanced CO oxidation activity. Wu *et al.* reported monodispersed CoPd bimetallic nanoparticle catalysts for CO oxidation.[24] Co-existed Pd and CoO_x on the surface promoted the CO oxidation activity because lattice oxygen atoms which are provided from CoO_x can react with adsorbed CO.

In this work, we report that Pd-based bimetallic catalysts were synthesized by deposition–precipitation method with addition of transition metals of Fe, Ni, and Co. The Pd-based bimetallic catalysts were significantly re-dispersed by hydrothermal treatment. The hydrothermally treated Pd-based bimetallic catalysts were employed to CO oxidation. The effects of the hydrothermal treatment and secondary metal species on Pd-based bimetallic catalysts were investigated using various analyses.

Experimental

Catalyst synthesis

Ceria was synthesized by precipitation method. 1 g of cerium nitrate ($Ce(NO_3)_3 \cdot 6H_2O$, Kanto Chemical) was dissolved in 24 mL of deionized (DI) water in a 250 mL round-bottom flask. Next, ammonia water (NH_4OH, Duksan) was injected dropwise and the pH of the solution was controlled until 8.7. The solution was stirred at 550 rpm for 1 h and then, it was turned to yellow slurry. The slurry was filtered and washed several times using DI water. Filtered precipitate was dried in convection oven at 80 °C overnight and pulverized using ceramic mortar. The powder was calcined at 500 °C for 5 h in static air.

Pd-based bimetallic catalysts ($PdFe/CeO_2$, $PdNi/CeO_2$, and $PdCo/CeO_2$) were synthesized by deposition–precipitation method. H_2MCl_4 (M = Pd, Fe, Ni, or Co) precursor solution was prepared with HCl solution. 2.5 mg of $PdCl_2$ (99%, Sigma-Aldrich), 3.5 mg of $FeCl_2$ (98%, Sigma-Aldrich), 6.1 mg of $NiCl_2 \cdot 6H_2O$ (ReagentPlus® grade, Sigma-Aldrich), or 6.2 mg of $CoCl_2 \cdot 6H_2O$ (98%, Sigma-Aldrich) was dissolved in 1 mL of DI water and mixed with HCl with a 1 : 2 molar ratio of metal to HCl. H_2PdCl_4 solution was homogeneously mixed with H_2FeCl_4, H_2NiCl_4, or H_2CoCl_4 solution to make Pd-based bimetallic catalysts. Na_2CO_3 solution was prepared using 530 mg of Na_2CO_3 powder and 20 mL of DI water. Ceria powder 300 mg was dispersed in 5 mL of DI water, and it was mixed with bimetallic metal precursor solution. Then Na_2CO_3 solution were added to the ceria solution simultaneously until pH reached 9. The solution was stirred at 800 rpm for 2 h and aged without stirring for 2 h. Then, the solution was filtered and washed with DI water and dried in convection oven at 80 °C for 5 h. Finally, dried powder was pulverized using ceramic mortar. For single phase Pd/CeO_2 catalyst, H_2PdCl_4 solution was introduced without mixing with other metal precursor solution. Other synthetic procedures were the same as the method for the bimetallic catalysts.

For re-dispersion of the Pd/CeO_2 and Pd-based bimetallic catalysts, hydrothermal treatment was performed for each catalyst. The catalyst powder was treated in a U-tube quartz cell with 144.5 sccm of air containing 10% H_2O at 750 °C for 25 h. After hydrothermal treatment, each catalyst powder was collected and denoted as Pd/CeO_2-HT, $PdFe/CeO_2$-HT, $PdCo/CeO_2$-HT, and $PdNi/CeO_2$-HT.

Characterizations

X-ray diffractometer (XRD) patterns of the catalysts were measured using SmartLab (Rigaku, Japan). Inductively coupled plasma-optical emission spectrometer (ICP-OES) was used for measuring the actual metal contents with iCAP 6300 Duo (Thermo Scientific, UK). Brunauer–Emmett–Teller (BET) surface area of the catalysts was measured using a TriStar II 3020 (Micromeritics, USA). All samples were degassed at 200 °C for 2 h to make a high vacuum before BET measurement. *In situ* diffuse reflectance infrared Fourier transform (DRIFT) spectroscopy was conducted using a Nicolet iS-50 instrument (Thermo Scientific, UK). 20 mg of each catalyst was mixed and ground with 180 mg of KBr powder. The mixed sample was put into a sample cup and it was set in the DRIFT cell. The cell was purged using Ar flow at 100 °C for 1 h to remove moisture and then cooled to room temperature. The DRIFT cell was charged with 1.5% CO gas with Ar balance (100 sccm) for 10 min, and then the DRIFT spectra were collected under vacuum to exclude the gaseous CO peaks. Extended X-ray absorption fine structure (EXAFS) and X-ray absorption near-edge structure (XANES) analysis were carried out at the 10C Wide XAFS beamline at Pohang Accelerator Laboratory (PAL).

Temperature-programmed desorption (TPD) of CO and CO_2 were performed using a BELCAT-B (BEL, Japan) equipped with a thermal conductivity detector. Each catalyst was loaded and treated with He flow at 200 °C for 2 h. The catalyst was cooled to room temperature under He flow, and then exposed to 10% CO/He flow for 1 h. After physically adsorbed CO was purged out by He flow at room temperature for 1 h, the sample was heated to 800 °C at a ramping rate of 10 °C min^{-1}. CO_2-TPD was conducted with the same pre-treatment method, and then pure CO_2 gas was introduced instead of 10% CO gas. Other methods were the same between CO-TPD and CO_2-TPD.

Metal dispersion was determined by modified CO chemisorption method of Takeguchi *et al.*[25] First, 50 mg of catalyst was heated under He gas at 200 °C for 10 min, and then the sample was reduced under a 4.9% H_2/Ar flow to 200 °C. After the sample was cooled to 50 °C, it was exposed to the following gas flow: (1) He (5 min); (2) 3.5% O_2/He (5 min); (3) CO_2 (10 min); (4) He (20 min); (5) 5% H_2/Ar (5 min). Then, CO pulse was injected every 1 min until the adsorption of CO onto the sample was saturated. Over-estimating the metal dispersion, which might be caused by CO adsorption on a ceria support as a carbonate, was prevented by CO_2 flow.

CO oxidation reaction

CO oxidation was carried out in a fixed bed U-tube quartz reactor. 50 mg of each catalyst was employed for CO oxidation. Reactant gas flow was introduced at a total flow rate of 100 sccm (1% CO and 1% O_2 in He balance) with 120 000 mL h^{-1} g_{cat}^{-1} of gas hourly space velocity. The reactor was heated to the target temperature with a ramping rate of 5 °C min^{-1} and held each temperature for 10 min to reach a steady-state. Reactants and

Open Access Article. Published on 13 January 2021. Downloaded on 2/8/2026 1:19:41 PM.
This article is licensed under a Creative Commons Attribution-NonCommercial 3.0 Unported Licence.

products were monitored by online gas chromatography system (GC 6500, Younglin) equipped with packed bed carboxen 1000 column (75035, SUPELCO, 15 ft × 1/8 in. × 2.1 mm) and thermal conductivity detector.

Results and discussion

Re-dispersion of Pd-based bimetallic catalysts

The changes of physicochemical properties of as-made and hydrothermally treated Pd-based catalysts were evaluated using BET surface area and metal dispersion as shown in Table 1. The BET isotherms of $PdFe/CeO_2$ are shown in Fig. S1.† The BET surface area of each catalyst decreased after hydrothermal treatment at 750 °C. The changes in metal dispersion after hydrothermal treatment were estimated using CO chemisorption analysis. The metal dispersion, which indicates the ratio of surface exposed metal atoms to total metal atoms, increased notably after hydrothermal treatment at 750 °C, indicating the re-dispersion of metal species while preventing the aggregation. The Pd size was estimated from the dispersion. The size of Pd nanoparticles decreased from 2.4 nm to 1.5 nm in Pd/CeO_2 and from 1.8 nm to 1.3 nm in $PdFe/CeO_2$ catalysts. The results of the ICP analysis in Table 1 show that all the as-made and hydrothermally treated Pd-based bimetallic catalysts have the similar metal contents of ~0.5 wt% of Pd and transition metals.

CO-DRIFTS experiments were carried out to investigate the surface metal structures over Pd/CeO_2 and Pd-based bimetallic catalysts. Fig. 1 shows the DRIFT spectra of adsorbed CO on as-made and hydrothermally treated Pd-based catalysts. CO is adsorbed linearly on an atop site of single Pd atom (2000–2200 cm^{-1}), and also on ensemble Pd sites with a bridge mode (1900–2000 cm^{-1}) and a threefold hollow mode (1800–1900 cm^{-1}).[26] The as-made Pd/CeO_2 and Pd-based bimetallic samples mainly exhibited hollow CO peak and bridge CO peak. However, the peak for linear CO adsorption increased significantly after hydrothermal treatment over all the samples, indicating the re-dispersion of metal species. CO-DRIFT experiments were also carried out using CeO_2 supported catalysts with only transition metals, and any peak for CO adsorption was not found on the transition metal.

As shown in the high angle annular dark field-scanning transmission electron microscopy (HAADF-STEM) and energy dispersive X-ray spectroscopy (EDS) mapping images (Fig. 2 and S2–S4†), Pd and transition metal species in as-made catalysts were highly dispersed on CeO_2 supports. In addition, hydrothermally treated catalysts also showed the highly dispersed Pd and transition metal species, similar to the initial state of metal distribution without any aggregated particles. Only the domain size of CeO_2 increased slightly after hydrothermal treatment.

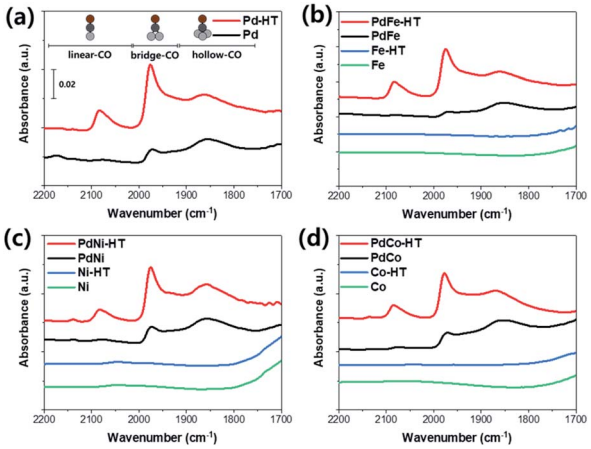

Fig. 1 CO-DRIFT spectra using as-made and hydrothermally treated (a) Pd, (b) PdFe, (c) PdNi, and (d) PdCo catalysts.

XRD patterns (Fig. S5†) of all as-made and hydrothermally treated Pd based catalysts in the range of 20°–80° were similar and matched well with the standard peak of CeO_2 (ICDD file no. 01-080-5548). There was no peak from metal particles, indicating that the metal species were highly dispersed in a small size on CeO_2 supports. The peak of CeO_2 became sharper after hydrothermal treatment, indicating that the CeO_2 domain size increased. These results are consistent with the BET surface area and TEM results. Overall, Pd-based bimetallic catalysts supported on CeO_2 are re-dispersed by hydrothermal treatment.

Catalytic performance

As shown in Fig. 3, the catalytic activity of Pd/CeO_2 and Pd-based bimetallic catalysts with various transition metals was estimated for CO oxidation. T_{100} values (the temperatures when CO conversion reached 100%) and light-off curves were compared. For Pd/CeO_2 catalysts, the light-off activity at low temperature was slightly improved after hydrothermal

Table 1 ICP results of as-made Pd-based catalysts, and BET surface area and CO uptake results of as-made and hydrothermally treated Pd-based catalysts. The Pd size was estimated from dispersion

		CeO_2	Pd/CeO_2	$PdFe/CeO_2$	$PdNi/CeO_2$	$PdCo/CeO_2$
Metal content (wt%)	Pd	—	0.4	0.4	0.4	0.4
	Fe/Ni/Co	—	—	0.5	0.5	0.5
BET surface area (m^2 g^{-1})	As-made	58.0	56.9	51.2	61.8	60.5
	After HT	20.0	24.6	22.2	28.5	20.8
Dispersion (%)	As-made	—	45.6	61.3	55.9	64.9
	After HT	—	75.1	86.7	87.4	88.0
Pd size (nm)	As-made	—	2.4	1.8	2.0	1.7
	After HT	—	1.5	1.3	1.3	1.3

© 2021 The Author(s). Published by the Royal Society of Chemistry

Open Access Article. Published on 13 January 2021. Downloaded on 2/8/2026 1:19:41 PM.
This article is licensed under a Creative Commons Attribution-NonCommercial 3.0 Unported Licence.

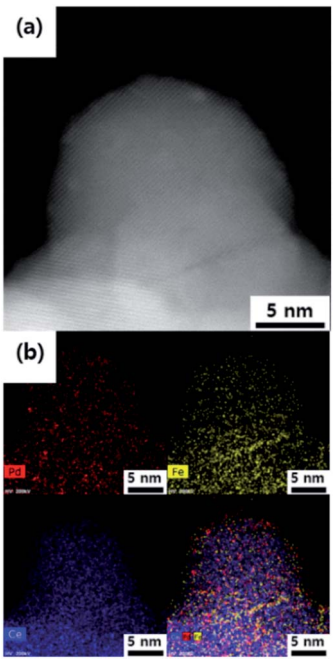

Fig. 2 (a) HAADF-STEM and (b) EDS mapping images of hydrothermally treated $PdFe/CeO_2$.

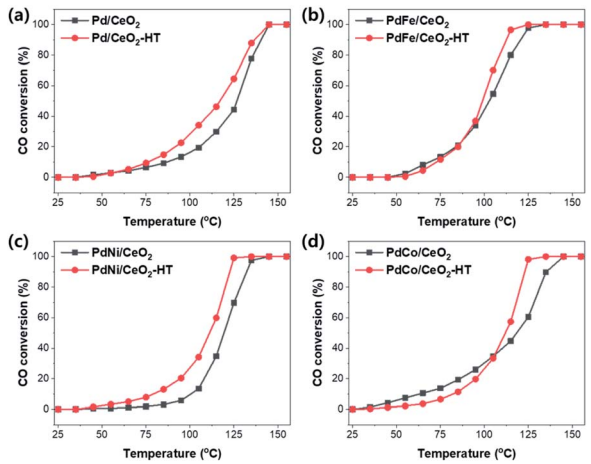

Fig. 3 CO oxidation results using as-made and hydrothermally treated bimetallic Pd-based catalysts using different transition metals; (a) Pd, (b) PdFe, (c) PdNi, and (d) PdCo (reaction condition: 50 mg of catalyst, 120 000 mL h^{-1} g_{cat}^{-1}, 100 sccm of total feed flow, 1% CO, 1% O_2, and 98% He).

treatment, but they exhibited same T_{100} values of 145 °C. After the addition of secondary transition metal species, however, the CO oxidation activity was improved with lower T_{100} value. In addition, when the Pd-based bimetallic catalysts were hydrothermally treated, the CO oxidation activity was further enhanced. T_{100} of $PdFe/CeO_2$ and $PdFe/CeO_2$-HT were 135 °C and 125 °C, respectively. In the case of $PdNi/CeO_2$ and $PdCo/CeO_2$ catalysts, CO oxidation activities were also enhanced after the hydrothermal treatment compared with the result of Pd/CeO_2 and Pd/CeO_2-HT, although their activity was lower than $PdFe/CeO_2$. The CO oxidation was also carried out using the catalysts containing only transition metals, and the results showed the lower activity (T_{100} > 200 °C) as shown in Fig. S6.†

The catalytic repeatability was tested for $PdFe/CeO_2$-HT catalyst. The light-off experiment was repeated 4 times (Fig. S7†), and the catalytic activity decreases by shifting to the right. The spent catalyst was regenerated by the hydrothermal treatment again at 750 °C for 25 h using 10% H_2O/air flow. The activity of the regenerated catalyst was restored to a similar level of the initial activity.

The adsorption strength of CO and CO_2 on the as-made and hydrothermally treated catalysts was estimated by CO-TPD and CO_2-TPD. The CO-TPD results of the Pd/CeO_2 and Pd-based bimetallic catalysts were shown in Fig. 4. The temperature of CO desorption decreased after hydrothermal treatment, indicating that the interaction of CO molecules with ceria surface became weaker, probably resulting from the re-dispersion of Pd species.[27] In particular, for $PdFe/CeO_2$ catalysts, the temperature of CO desorption showed the lowest value of 91 °C after hydrothermal treatment. CO_2-TPD was also conducted and the temperature of CO_2 desorption also decreased after hydrothermal treatment as shown in Fig. 5. In the CO oxidation mechanism, facile CO_2 desorption is an important step to achieve the high activity at low temperature.[28] The CO_2 desorption temperature of $PdFe/CeO_2$-HT catalyst showed the lowest value of 87 °C. In addition, the peak area of CO_2 desorption was much smaller after the hydrothermal treatment in all cases. Facile CO_2 desorption after hydrothermal treatment is an important factor to improve the CO oxidation activity.

XANES analysis was conducted over the Pd/CeO_2 and Pd-based bimetallic catalysts to determine the change in Pd oxidation state before and after hydrothermal treatment. As shown in Fig. 6a, all of the as-made and hydrothermally treated samples had similar Pd oxidation state of the intermediate stage between Pd foil and PdO references. Pd K edge EXAFS data of Pd/CeO_2 and $PdFe/CeO_2$ before and after hydrothermal treatment were described with PdO and Pd foil (Fig. 6b), and

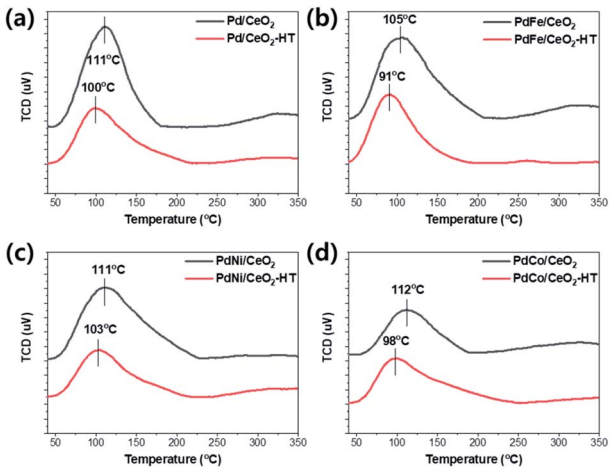

Fig. 4 CO-TPD results using as-made and hydrothermally treated (a) Pd/CeO_2, (b) $PdFe/CeO_2$, (c) $PdNi/CeO_2$, and (d) $PdCo/CeO_2$ catalysts.

Open Access Article. Published on 13 January 2021. Downloaded on 2/8/2026 1:19:41 PM.
This article is licensed under a Creative Commons Attribution-NonCommercial 3.0 Unported Licence.

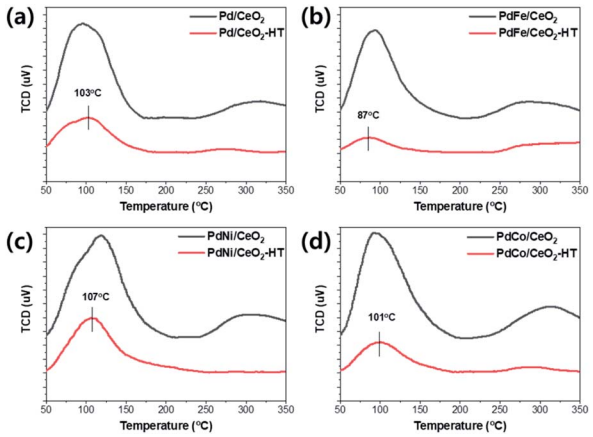

Fig. 5 CO_2-TPD results using as-made and hydrothermally treated (a) Pd/CeO_2, (b) $PdFe/CeO_2$, (c) $PdNi/CeO_2$, and (d) $PdCo/CeO_2$ catalysts.

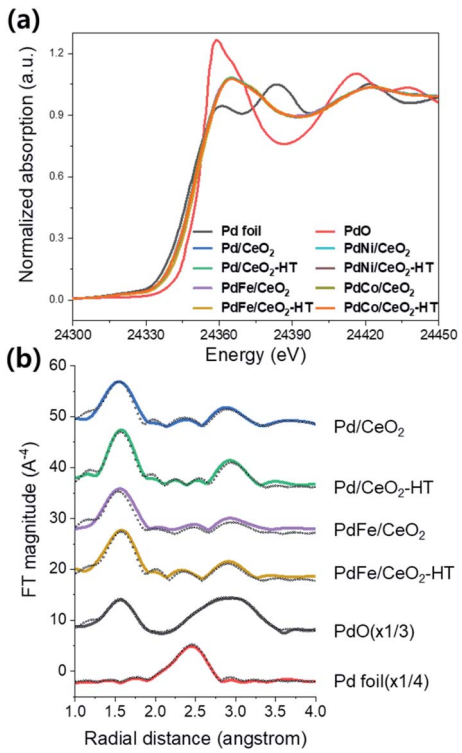

Fig. 6 (a) Pd K edge XANES spectra of as-made and hydrothermally treated bimetallic Pd based catalysts using different transition metals. (b) Pd K edge k^3-weighted Fourier transformed EXAFS spectra of Pd/CeO_2 and $PdFe/CeO_2$ catalyst before and after hydrothermal treatment. The dots indicate fitted results, and lines indicate experimental data.

their fitting results are shown in Table 2. The coordination number of Pd–Pd and Pd–O–Pd decreased from 0.8 and 0.9 to 0.0 and 0.2, respectively after hydrothermal treatment in the case of Pd/CeO_2. On the other hand, the coordination number for Pd–O–Ce increased from 1.6 to 2.7 after hydrothermal treatment. It indicates that the Pd species were re-dispersed, and the coordination of Pd with CeO_2 increased after

Table 2 EXAFS fitting data of as-made and hydrothermally treated Pd/CeO_2 and $PdFe/CeO_2$ catalysts

Sample	Path	Coordination number (R)	Interatomic distance (Å)
Pd/CeO_2	Pd–O	2.4 ± 0.4	1.98 ± 0.02
	Pd–Pd	0.8 ± 0.2	2.72 ± 0.01
	Pd–O–Ce	1.6 ± 0.5	3.20 ± 0.03
	Pd–O–Pd	0.9 ± 0.2	3.48 ± 0.04
Pd/CeO_2-HT	Pd–O	3.0 ± 0.3	1.99 ± 0.03
	Pd–Pd	0.0 ± 0.0	2.72 ± 0.02
	Pd–O–Ce	2.7 ± 0.3	3.22 ± 0.02
	Pd–O–Pd	0.2 ± 0.2	3.47 ± 0.01
$PdFe/CeO_2$	Pd–O	2.3 ± 0.4	2.00 ± 0.02
	Pd–Fe	0.0 ± 0.0	2.62 ± 0.02
	Pd–Pd	0.4 ± 0.1	2.74 ± 0.02
	Pd–O–Ce	1.5 ± 0.5	3.22 ± 0.03
	Pd–O–Pd	0.5 ± 0.0	3.48 ± 0.01
$PdFe/CeO_2$-HT	Pd–O	2.5 ± 0.3	1.99 ± 0.02
	Pd–Fe	1.3 ± 0.2	2.62 ± 0.03
	Pd–Pd	0.0 ± 0.0	2.74 ± 0.01
	Pd–O–Ce	1.7 ± 0.4	3.21 ± 0.03
	Pd–O–Pd	0.3 ± 0.1	3.48 ± 0.02

hydrothermal treatment. For $PdFe/CeO_2$, the coordination number of Pd–Pd and Pd–O–Pd decreased from 0.4 and 0.5 to 0.0 and 0.3, respectively, after hydrothermal treatment. Notably, the interaction of Pd–Fe newly appeared with coordination number of 1.3 after hydrothermal treatment. $PdNi/CeO_2$ and $PdCo/CeO_2$ also had the coordination number of Pd–Ni (1.1) and Pd–Co (0.9) after hydrothermal treatment, as shown in Fig. S8 and S9 and Table S1.† The hydrothermal treatment induced the metal re-dispersion, and also made the interaction of Pd-transition metal in Pd-based bimetallic catalysts.

CO was adsorbed on Pd sites in bimetallic catalysts, as confirmed by CO-DRIFT in Fig. 1. In general, it is assumed that CO oxidation follows Mars–van Krevelen mechanism, by which CO directly reacts with the surface oxygen, producing CO_2 and leaving behind surface oxygen vacancies which are then filled with gaseous O_2.[29] The transition metal sites in bimetallic catalysts have the high oxygen affinity and possibly act as O_2 dissociation sites to enhance CO oxidation reaction.[30] The activity of $PdFe/CeO_2$-HT catalyst for CO oxidation was compared with literature values in Table S2,† indicating that the $PdFe/CeO_2$-HT showed good activity compared to other works.

Conclusion

Pd/CeO_2 and CeO_2-supported Pd-based bimetallic catalysts were prepared by deposition–precipitation method using various transition metals of Fe, Ni, Co. CO-DRIFT spectra, CO chemisorption, and HAADF-STEM results showed that metal species were re-dispersed on the CeO_2 support without aggregation after hydrothermal treatment, resulting in highly dispersed metal. Pd-based bimetallic catalysts showed the higher activity than Pd/CeO_2 for CO oxidation, and the activities were further enhanced after hydrothermal treatment due to metal re-dispersion. $PdFe/CeO_2$-HT showed the highest catalytic

© 2021 The Author(s). Published by the Royal Society of Chemistry

Open Access Article. Published on 13 January 2021. Downloaded on 2/8/2026 1:19:41 PM.
This article is licensed under a Creative Commons Attribution-NonCommercial 3.0 Unported Licence.

activity with lowest T_{100} value of 125 °C. Results of CO-TPD, CO_2-TPD, and EXAFS also indicated the re-dispersion of metal species after hydrothermal treatment. CO and CO_2 molecules were desorbed at lower temperature after hydrothermal treatment due to highly dispersed metal species by re-dispersion. From EXAFS data, the coordination of Pd and transition metal appeared after hydrothermal treatment, indicating the interaction of Pd with transition metal in Pd-based bimetallic catalysts. Re-dispersion of metal species and the interaction of Pd with transition metal in bimetallic catalysts upon the hydrothermal treatment enabled high activity for CO oxidation.

Conflicts of interest

There are no conflicts to declare.

Acknowledgements

This research was supported by Korea Institute of Machinery and Materials (NK225E).

References

1 S. J. Tauster, S. C. Fung, R. T. K. Baker and J. A. Horsley, *Science*, 1981, **211**, 1121–1125.
2 N. Tiengchad, O. Mekasuwandumrong, C. Na-Chiangmai, P. Weerachawanasak and J. Panpranot, *Catal. Commun.*, 2011, **12**, 910–916.
3 M. Cargnello, V. V. T. Doan-Nguyen, T. R. Gordon, R. E. Diaz, E. A. Stach, R. J. Gorte, P. Fornasiero and C. B. Murray, *Science*, 2013, **341**, 771–773.
4 D. Pakhare and J. Spivey, *Chem. Soc. Rev.*, 2014, **43**, 7813–7837.
5 K. Yu, L. L. Lou, S. X. Liu and W. Z. Zhou, *Adv. Sci.*, 2020, **7**, 1901970.
6 P. Y. Xin, J. Li, Y. Xiong, X. Wu, J. C. Dong, W. X. Chen, Y. Wang, L. Gu, J. Luo, H. P. Rong, C. Chen, Q. Peng, D. S. Wang and Y. D. Li, *Angew. Chem., Int. Ed.*, 2018, **57**, 4642–4646.
7 Z. Wang, Z. P. Qu, X. Quan, Z. Li, H. Wang and R. Fan, *Appl. Catal., B*, 2013, **134**, 153–166.
8 H. L. Wang, S. T. Luo, M. S. Zhang, W. Liu, X. D. Wu and S. Liu, *J. Catal.*, 2018, **368**, 365–378.
9 G. Spezzati, A. D. Benavidez, A. T. DeLaRiva, Y. Q. Su, J. P. Hofmann, S. Asahina, E. J. Olivier, J. H. Neethling, J. T. Miller, A. K. Datye and E. J. M. Hensen, *Appl. Catal., B*, 2019, **243**, 36–46.
10 P. Granger and V. I. Parvulescu, *Chem. Rev.*, 2011, **111**, 3155–3207.
11 J. H. Wang, H. Chen, Z. C. Hu, M. F. Yao and Y. D. Li, *Catal. Rev.*, 2015, **57**, 79–144.
12 J. F. Rodriguez and W. K. Cheng, *SAE Int. J. Engines*, 2017, **10**, 646–655.
13 U. Shamraiz, Z. Ahmad, B. Raza, A. Badshah, S. Ullah and M. A. Nadeem, *ACS Appl. Mater. Interfaces*, 2020, **12**, 4396–4404.
14 Y. Z. Li, Y. Yu, J. G. Wang, J. Song, Q. Li, M. D. Dong and C. J. Liu, *Appl. Catal., B*, 2012, **125**, 189–196.
15 J. H. Kang, E. W. Shin, W. J. Kim, J. D. Park and S. H. Moon, *J. Catal.*, 2002, **208**, 310–320.
16 L. Rodriguez, D. Romero, D. Rodriguez, J. Sanchez, F. Dominguez and G. Arteaga, *Appl. Catal., A*, 2010, **373**, 66–70.
17 Y. Nishihata, J. Mizuki, T. Akao, H. Tanaka, M. Uenishi, M. Kimura, T. Okamoto and N. Hamada, *Nature*, 2002, **418**, 164–167.
18 J. Y. Luo, M. Meng, X. Li, X. G. Li, Y. Q. Zha, T. D. Hu, Y. N. Xie and J. Zhang, *J. Catal.*, 2008, **254**, 310–324.
19 Y. Nagai, K. Dohmae, Y. Ikeda, N. Takagi, T. Tanabe, N. Hara, G. Guilera, S. Pascarelli, M. A. Newton, O. Kuno, H. Y. Jiang, H. Shinjoh and S. Matsumoto, *Angew. Chem., Int. Ed.*, 2008, **47**, 9303–9306.
20 S. Kaneko, M. Izuka, A. Takahashi, M. Ohshima, H. Kurokawa and H. Miura, *Appl. Catal., A*, 2012, **427–428**, 85–91.
21 H. Jeong, J. Bae, J. W. Han and H. Lee, *ACS Catal.*, 2017, **7**, 7097–7105.
22 T. A. Yamamoto, T. Nakagawa, S. Seino and H. Nitani, *Appl. Catal., A*, 2010, **387**, 195–202.
23 B. Liu, Z. Zhao, G. Henkelman and W. Y. Song, *J. Phys. Chem. C*, 2016, **120**, 5557–5564.
24 C. H. Wu, C. Liu, D. Su, H. L. L. Xin, H. T. Fang, B. Erens, S. Zhang, C. B. Murray and M. B. Salmeron, *Nat. Catal.*, 2019, **2**, 78–85.
25 T. Takeguchi, S. Manabe, R. Kikuchi, K. Eguchi, T. Kanazawa, S. Matsumoto and W. Ueda, *Appl. Catal., A*, 2005, **293**, 91–96.
26 C. Wang, C. Wen, J. Lauterbach and E. Sasmaz, *Appl. Catal., B*, 2017, **206**, 1–8.
27 C. Lemire, R. Meyer, S. K. Shaikhutdinov and H. J. Freund, *Surf. Sci.*, 2004, **552**, 27–34.
28 M. Huang and S. Fabris, *J. Phys. Chem. C*, 2008, **112**, 8643–8648.
29 Z. L. Wu, M. J. Li and S. H. Overbury, *J. Catal.*, 2012, **285**, 61–73.
30 R. T. Mu, Q. A. Fu, H. Xu, H. I. Zhang, Y. Y. Huang, Z. Jiang, S. O. Zhang, D. L. Tan and X. H. Bao, *J. Am. Chem. Soc.*, 2011, **133**, 1978–1986.

© 2021 The Author(s). Published by the Royal Society of Chemistry